

# A SPHERICAL COUETTE EXPERIMENT TO OBSERVE INDUCTION-LESS MHD INSTABILITIES AT MEDIUM REYNOLDS NUMBERS

Elliot Kaplan<sup>1,\*</sup>, Benjamin Gohl<sup>1</sup>, Martin Seilmayer<sup>1</sup>, and Frank Stefani<sup>1</sup>

<sup>1</sup>Helmholtz-Zentrum Dresden-Rossendorf—Bautzner Landstraße 400—01328  
Dresden—Germany

\*e.kaplan@hzdr.de

**Abstract:** A liquid metal (GaInSn) spherical Couette flow is being carried out at the Helmholtz-Zentrum in Dresden-Rossendorf to explore a region of Reynolds-Hartmann space in which numerical simulations [1, 2] show hydrodynamically unstable and magnetohydrodynamically unstable regions separated by an isthmus of stability. The region is of further interest because these (inductionless) instabilities have similar signatures to the instabilities found in a larger scale, less thoroughly diagnosed experiment, that were reported as the (induction dependent) Magnetorotational instability (MRI) [3].

## 1. Introduction

Two spheres, one inside the other, in differential rotation with a layer of fluid between will generate a broad array of possible dynamics in the enclosed fluid, depending on the aspect ratio, the rotation rates of the spheres, and the viscosity of the fluid. If the fluid is electrically conducting and permeated by a magnetic field, applied and/or self-excited, the array of possible dynamics broadens further. The configuration, known as magnetized spherical Couette flow, was first studied numerically by Hollerbach [4] as an extension of the nonmagnetic spherical Couette problem [5, 6]. Since then the flow has been investigated, numerically [1, 7–9] and experimentally [3, 10], under a variety of imposed fields and magnetic boundary conditions. A compendium of magnetized spherical Couette results can be found in [11].

A long, albeit contentiously, discussed result of magnetized spherical Couette flow was the observation of an angular momentum transporting, magnetically induced instability in a turbulent (Reynolds number  $\text{Re} \approx 10^7$ , where  $\text{Re} = r_1^2 \Omega / \nu$ , with  $r_1$  inner radius,  $\Omega$  inner sphere rotation rate, and  $\nu$  bulk viscosity of the fluid) liquid metal flow, which was described in [3] as the long sought-after Magnetorotational Instability (MRI). In contrast to the MRI as usually described [12], this instability was non-axisymmetric and demonstrated an equatorial symmetry whose parity depended on the strength of the applied magnetic field. Subsequent numerical investigations [1, 7] turned up a collection of induction-free instabilities—related to the hydrodynamic jet instability, the Kelvin-Helmholtz-like Shercliff instability, and a return flow instability—that replicated the parity properties, as well as the torque on the outer sphere (the proxy measurement of angular momentum transport). A more modestly scaled ( $\text{Re} < 10^5$ ), but more comprehensively diagnosed (Ultrasonic Doppler Velocimetry (UDV), electric potential measurements), spherical Couette experiment is being carried out at the Helmholtz-Zentrum Dresden-Rossendorf in order to better characterize these instabilities, their criteria, and their saturation. Presented here are initial data from the experiment, as well as some phenomenology of the saturation and bifurcation of the instabilities via nonlinear transfer of energy between azimuthal modes as revealed by the numerical simulations.

## 2. Simulation

Preliminary simulation of the experiment was carried out using a code, described in [13], that solves for a flow, driven by the rotating inner sphere, according to the incompressible Navier-Stokes Equation:

$$\nabla \cdot \mathbf{U} = 0, \quad \nabla \times \mathbf{U} = \boldsymbol{\omega}, \quad \partial \boldsymbol{\omega} / \partial t = \nabla \times \mathbf{F} + \nabla^2 \boldsymbol{\omega}. \quad (1)$$

The body force  $\mathbf{F}$  is given by

$$\mathbf{F} = \text{Re} (\nabla \times \mathbf{U}) \times \mathbf{U} + \text{Ha}^2 (\nabla \times \mathbf{B}) \times \mathbf{B}, \quad (2)$$

with  $\mathbf{U}$  and  $\mathbf{B}$  vector fields of the velocity and magnetic fields respectively, and  $\text{Ha}$  the Hartmann number ( $B_0 r_1 \sqrt{\sigma / \rho \nu}$ ,  $B_0$  applied field strength,  $\sigma$  electrical conductivity,  $\rho$  mass density).

The magnetic field is split into an applied ( $\mathbf{B}_0$ ) and an induced ( $\mathbf{b}$ ) component, where the applied field is curl free within the flow domain. The Lorentz force is then given by

$$(\nabla \times \mathbf{B}) \times \mathbf{B} = (\nabla \times \mathbf{b}) \times \mathbf{B}_0 + (\nabla \times \mathbf{b}) \times \mathbf{b}, \quad (3)$$

where  $\mathbf{b}$  is given by the magnetic induction equation in the (so-called inductionless) limit where diffusion ( $\nabla^2 \mathbf{b}$ ) exactly balances advection ( $\nabla \times (\mathbf{U} \times \mathbf{B}_0)$ ):

$$0 = \nabla^2 \mathbf{b} + \nabla \times (\mathbf{U} \times \mathbf{B}_0). \quad (4)$$

The  $((\nabla \times \mathbf{b}) \times \mathbf{b})$  term in Eqn. 3 is taken to be small. In all of the simulations performed in preparation for this experiment, the applied field was taken to be axial.

The simulations are run according to the following procedure. First a flow including only the axisymmetric modes is evolved to a steady state solution for given values of ( $\text{Re}$ ,  $\text{Ha}$ ). The linear stability of the  $m \neq 0$  harmonics are then tested through a linearized Navier-Stokes calculation. The unstable flows are then seeded with three-dimensional, nonaxisymmetric noise and evolved until the instability saturates. Figure 1a shows the stability boundaries for a flow with aspect ration 0.5. Figure 1b-d show energy densities of the instabilities associated flow of  $\text{Re}$  1000 and  $\text{Ha}$  10, 30 and 70 respectively, with streamlines of the axisymmetric meridional flow overlaid. Figure 1e-f shows the same with isocontours of the angular momentum. The values of  $\text{Re}$  and  $\text{Ha}$  are chosen because the actual instability takes on a different character in each. At low  $\text{Ha}$ , the instability arises in the jet (1b). At medium  $\text{Ha}$ , it arises in the stagnation point of the meridional flow (1c). At high  $\text{Ha}$ , it arises along the Shercliff Layer (1g).

The steady states of the full three-dimensional calculation have the practical use of guiding diagnostic design and expectations for the low  $\text{Re}$  cases (discussed further in Section 3. below). They also demonstrate a saturation mechanism for the instabilities [14].

## 3. Apparatus

The physical experiment consists of one of two possible inner spheres ( $r_1 = 3$  cm or 4.5cm) held in the center of an outer sphere ( $r_2 = 9$  cm). The outer sphere is a Polymethyl Methacrylate (PMMA) acrylic with cylindrical holders for ultrasonic doppler velocimetry (UDV), and perforations to admit copper electrodes for potential measurement. Figure 2a shows a Solidworks<sup>®</sup> model of the experiment including the diagnostics, Figure 2b shows the actual manufactured vessel. The space between the spheres is filled with a GaInSn eutectic alloy. Because of the high density of the medium (roughly 6 times that of water), each inner sphere holds a lead weight to counter the buoyancy force. The axial magnetic field is provided by a pair of copper

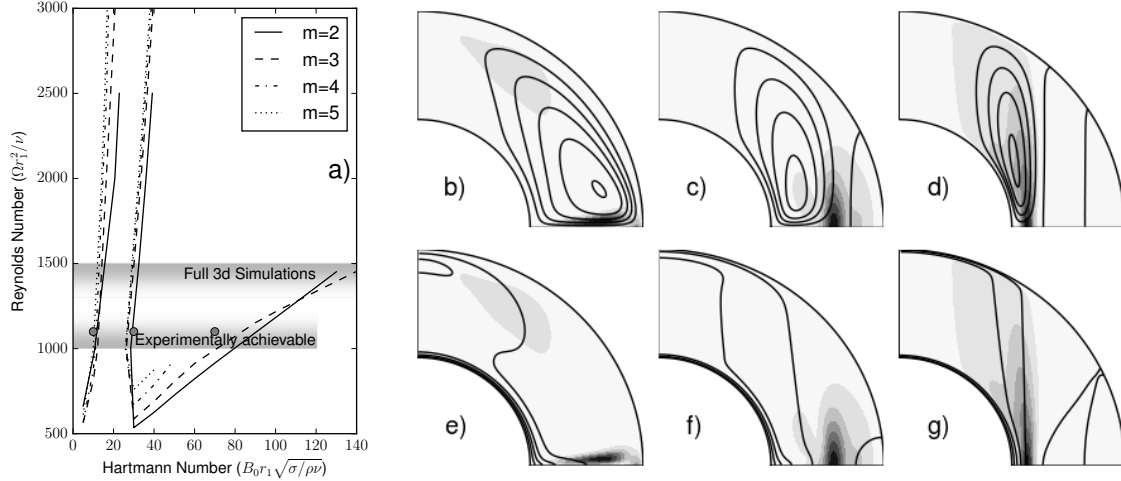


Figure 1: a) Critical Reynolds numbers as a function of Hartmann number for symmetric and antisymmetric instabilities calculated from a linearized Navier-Stokes equation analysis of the axisymmetric base flows. The boundaries of the region which can be reasonably simulated, and the region which can be reached in the experiment are indicated by the shaded bands. The (Ha, Re) values of the flows Figures b-g are indicated by circles. b-g). Profiles of the energy density of the most unstable eigenmode from at three different Hartmann numbers at Re 1100. b-d show streamlines of the meridional flow over the energy density of the  $m=2$  harmonic. e-g show contours of the angular momentum over the same. b and e show the equatorially antisymmetric jet instability (Re 1100, Ha 10). c and f show the equatorially symmetric return flow instability (Re 1100, Ha 30). d and g show the equatorially symmetric Shercliff layer instability (Re 1100, Ha 70).

electromagnets (not pictured) with central radii of 30 cm, with a vertical gap of 31 cm between them (a near Helmholtz configuration). The inner and outer spheres are driven with a minimum rotation frequency of  $\sim 0.02$  hz by a pair of 90 W electromotors connected to 100 x 1 gears. The electromagnets provide 1 mT of axial magnetic field (or 1.17 Ha) per 4.2 Amps through the coils.

The simulations of Section 2. provide estimates of the potential differences between electrodes and the velocities measured along the UDV chords. Table 1 shows a summary of these predictions, as well as engineering data, for the lowest Re runs of interest. At such low rotation rates, the peak velocity signals are on the order of a half mm/s for all three classes of instability, which can be reasonably measured using standard UDV probes. The potential differences are drastically different between the instabilities—the potential is a product of the background magnetic field and the flow—but even the lowest voltages are measurable when appropriately preamplified. The initial run campaigns of the experiment will seek to confirm the most interesting features of Fig. 1: the stability isthmus in the vicinity of Ha 20, the Reynolds line around Ha 30 where an increase in Re stabilizes the flow (in contradiction to typical intuition), and the transition between the three types on instability.

#### 4. Summary

As of the writing of this proceedings paper, the vessel, the test stand and the electromagnetic coils have all been manufactured. It remains to affix the diagnostics to the sphere and to attach

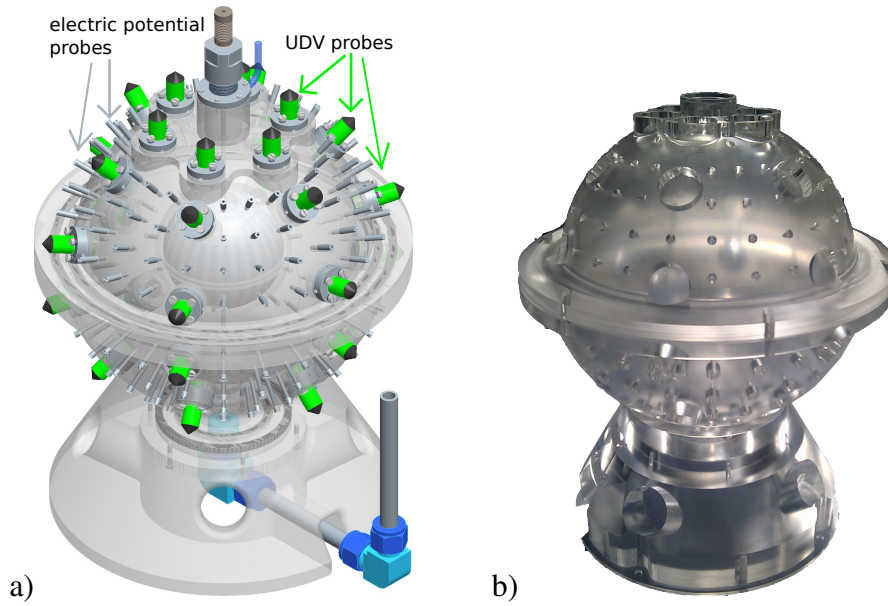


Figure 2: (A) Solidworks® model the spherical Couette experiment. Some UDV and potential probes are indicated in the figure. The elbowed tube is for the gallium fill. (B) real spherical vessel. Pits hold the real diagnostics.

the power and cooling supplies to the electromagnets.

## Acknowledgements

This work is supported by the Deutsche Forschungsgemeinschaft under grant STE 991/1-2.

## 5. References

- [1] Hollerbach, R. (2009). Non-axisymmetric instabilities in magnetic spherical Couette flow. *Proc. R. Soc. London A*, 465:2003–2013.
- [2] Travnikov, V.; Eckert, K.; and Odenbach, S.: (2011). Influence of an axial magnetic field on the stability of spherical Couette flows with different gap widths. *Acta Mech*, 219:255–268.
- [3] Sisan, D. R.; Mujica, N.; Tillotson, W. A.; Huang, Y.-M.; Dorland, W.; Hassam, A. B.; Antonsen, T. M.; and Lathrop, D. P.: (2004). Experimental Observation and Characterization of the Magnetorotational Instability. *Phys. Rev. Lett.*, 93(11):114502.
- [4] Hollerbach, R. (1994). Magnetohydrodynamic Ekman and Stewartson Layers in a Rotating Spherical Shell. *R. Soc. London Proc. Ser. A*, 444:333–346.

Reynolds	Hartmann	$\Omega_{in}$	$B_0$	$\bar{\phi}_{max}$	$\tilde{\phi}_{max}$	$\bar{v}_{max}$	$\tilde{v}_{max}$
1000	10	0.0235 Hz.	9 mT	10 $\mu$ V	367 nV	0.412 mm/s	0.305 mm/s
1000	30	0.0235 Hz.	26 mT	32 $\mu$ V	1.1 $\mu$ V	0.340 mm/s	0.331 mm/s
1000	70	0.0235 Hz.	60 mT	70 $\mu$ V	8.6 mV	0.067 mm/s	0.438 mm/s

Table 1: Predictions for diagnostic outputs for three typical run conditions. The mean potential ( $\bar{\phi}$ ) represents the time averaged potential difference between the pole and the equator. The fluctuating potential ( $\tilde{\phi}$ ) represents the largest amplitude potential difference between two points at a single latitude. The mean and fluctuating velocities are taken by projecting the simulated flow along a UDV chord. The max values over any probe is shown.

- [5] Stewartson, K. (1966). On almost rigid rotations. *J. Fluid Mech.*, 1:131–144.
- [6] Proudman, I. (1956). The almost-rigid rotation of viscous fluid between concentric spheres. *J. Fluid Mech.*, 1:505–516.
- [7] Gissinger, C.; Ji, H.; and Goodman, J.: (2011). Instabilities in magnetized spherical Couette flow. *Phys. Rev. E*, 84(2):026308.
- [8] Hollerbach, R. and Skinner, S.: (2001). Instabilities of magnetically induced shear layers and jets. *Proc. R. Soc. London A*, 457:785–802.
- [9] Dormy, E.; Jault, D.; and Soward, A. M.: (2002). A super-rotating shear layer in magnetohydrodynamic spherical Couette flow. *J. Fluid Mech.*, 452:263–291.
- [10] Nataf, H.-C.; Alboussière, T.; Brito, D.; Cardin, P.; Gagnière, N.; Jault, D.; and Schmitt, D.: (2008). Rapidly rotating spherical Couette flow in a dipolar magnetic field: An experimental study of the mean axisymmetric flow. *Physics of the Earth and Planetary Interiors*, 170:60–72.
- [11] Rüdiger, G.; Kitchatinov, L. L.; and Hollerbach, R.: (2013). *Magnetic Processes in Astrophysics*, pages 287–326. Wiley-VCH Verlag GmbH & Co. KGaA.
- [12] Balbus, S. A. and Hawley, J. F.: (1991). A powerful local shear instability in weakly magnetized disks. *Astrophys. J.*, 376:214–233.
- [13] Hollerbach, R. (2000). A spectral solution of the magneto-convection equations in spherical geometry. *Int. J. Numer. Meth. Fluids*, 32:773–797.
- [14] Kaplan, E. (2014). On the saturation of non-axisymmetric instabilities of magnetized spherical Couette flow. *ArXiv e-prints*: 1402.5064.